

The gravitational lensing nature of the Cloverleaf unveiled in CO (7-6) line emission[★]

D. Alloin¹, S. Guilloteau², R. Barvainis³, R. Antonucci⁴, and L. Tacconi⁵

¹ Service d'Astrophysique, CE Saclay, F-91191 Gif-sur-Yvette Cedex, France

² Institut de Radio Astronomie Millimétrique, 300 Rue de la Piscine, F-38406 Saint Martin d'Hères, France

³ MIT Haystack Observatory, Westford, MA 01886 USA

⁴ UC Santa Barbara, Physics Department, Santa Barbara, CA 93106 USA

⁵ Max Planck Institut für extraterrestrische Physik, D-85748 Garching Germany

Received 11 December 1996 / Accepted 27 February 1997

Abstract. We report 0.5'' resolution imaging of the Cloverleaf quasar in the CO(7-6) line and 1.3 mm continuum, as well as 1'' resolution imaging in the CO(3-2) line, performed with the IRAM interferometer. The CO(7-6) image is clearly resolved into 4 spots, demonstrating that the CO emission is also gravitationally lensed. We do not find any convincing evidence for a velocity gradient in the maps. As compared to the optical spots from a V band HST image, some of the CO spots are found to be stretched along the Einstein ring. Using the available lens model for the Cloverleaf, this suggests an intrinsic radius of ~ 600 pc for the CO emitting region. No continuum emission is detected: the measured flux density is 5 ± 3 mJy, consistent with a spectral index larger than 3.

Key words: quasars: H 1413+117 – gravitational lensing – radio lines: ISM

1. Introduction

The Cloverleaf, H1413+117 ($14^{\text{h}}15^{\text{m}}46^{\text{s}}.23$ $11^{\circ}29'44''.0$, J2000.0), was first identified as a gravitational lens with four spots by Magain et al. (1988). The spots, labeled A,B,C,D (see Fig. 1b), show separations in the range 0.77'' to 1.36''. Spectroscopic data confirmed that they are related to a single quasar at redshift 2.558. So far, the Cloverleaf has been observed in the following wavebands: B, V, R and I (Magain et al. 1988, Kayser et al. 1990, hereafter K90, Angonin et al. 1990, Arnould et al. 1993, Falco, 1993), at 2.2 μm (Lawrence 1996) and in the radio continuum at 3.6cm (K90). Although the lensing object itself has not been directly detected, these data sets allow further

specification of the properties of the gravitational lens system (K90). From an analysis of the light-curves, spot D is known to be affected by microlensing effects (Angonin et al. 1990; Remy et al. 1996).

Regarding the dust/molecular content of the quasar, the Cloverleaf has been detected in the CO (3-2) line (Barvainis et al. 1994, B94). In this early data set, the CO (3-2) line emission from the Cloverleaf was spatially unresolved with a beam size of $8.6'' \times 7.1''$. Subsequent observations with the BIMA interferometer did not resolve either the image in the CO(3-2) line with a $2.8'' \times 2.4''$ (Wilner et al. 1995). New observations with the IRAM 30-m telescope were performed to measure the line fluxes in several CO transitions, (3-2), (4-3), (5-4) and (7-6), as well as in at least one fine structure line of CI and possibly in the HCN (4-3) transition, leading to new constraints on the physical parameters of the warm gas responsible for the line emission (Barvainis et al. 1997, B97). Measurements of the Cloverleaf continuum in the range 25 to 1350 μm are presented and discussed in Barvainis et al. (1995, B95).

A CO(7-6) map has been obtained by Scoville et al. (1996) with OVRO, showing isophote deformations consistent with the optical configuration. However, neither the S/N of the map, nor the spatial resolution are high enough to separate unambiguously the spots. We report here on new measurements of the Cloverleaf using the IRAM interferometric array with baselines long enough to reach an angular resolution of about 0.5''. An advantage of deriving the macrolensing amplification factors from CO images is that the CO source should be sufficiently extended to be insensitive to microlensing effects. Thus we expect the macrolensing parameters derived from CO to provide a better representation of the lensing system. Finally, if the CO source in the quasar is extended, we expect to see different patterns for the CO lensed spots compared to the B, V, R, I spots which are likely to relate to a more compact core within the quasar. From these differences, we may even constrain the size of the CO source.

Send offprint requests to: D.Alloin

[★] Based on observations at the Institut de Radio Astronomie Millimétrique, supported by INSU/CNRS (France), MPG (Germany) and IGN (Spain)

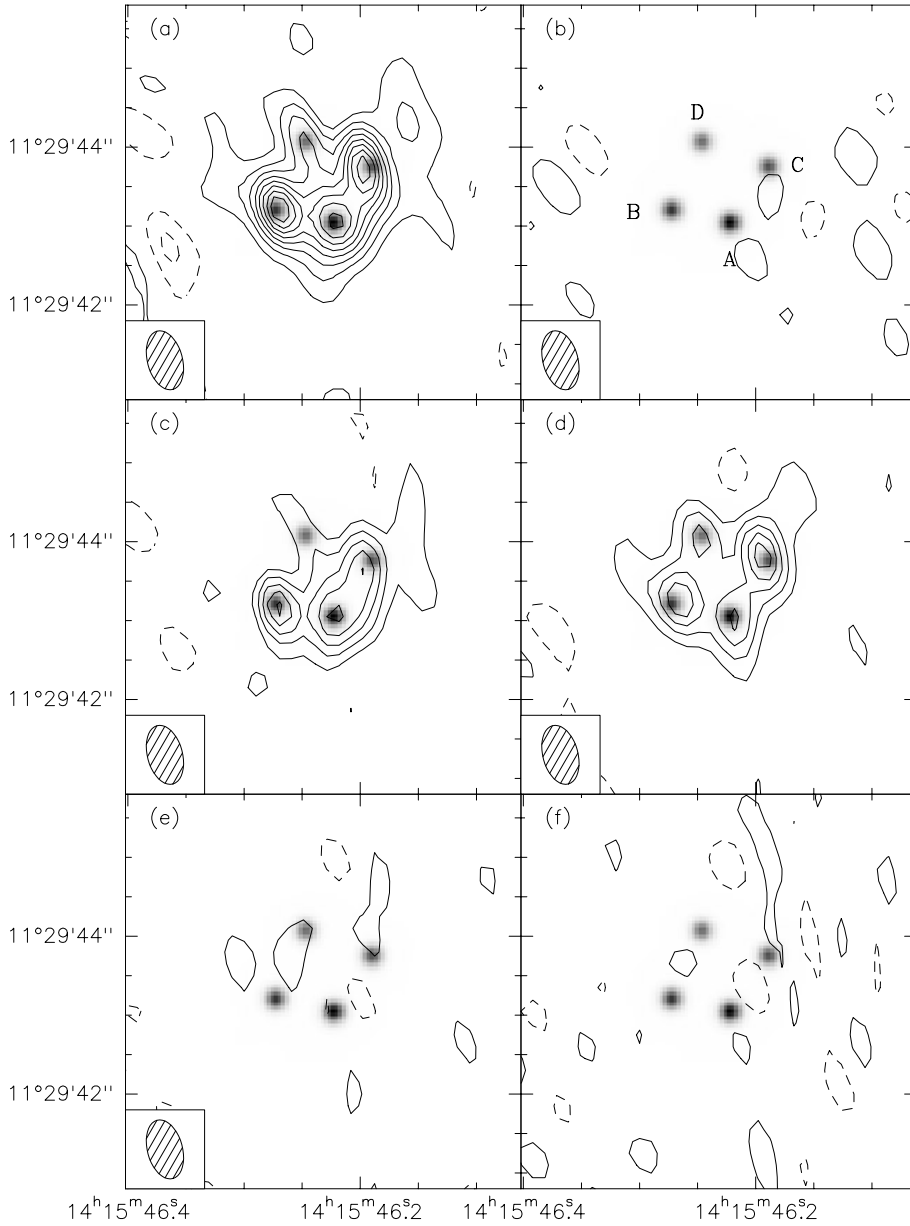


Fig. 1. **a** CO(7-6) map restored with the natural beam of $0.77'' \times 0.44''$ at PA 15° . Contour spacing is 1.65 mJy/beam (corresponding to 1.1 Jy.km.s^{-1}) i.e. 2σ . **b** 1.3 mm continuum map obtained from the image band. Contour spacing is 1.9 mJy/beam (2σ). **c** CO(7-6) map obtained over the blue-shifted part of the line (-325 to -75 km.s^{-1}). **d** CO(7-6) map obtained over the red-shifted part of the line (75 to 325 km.s^{-1}). Contour spacing is 2.7 mJy/beam (1.7 Jy.km.s^{-1} , 2σ) for **c** and **d**. **e** Difference between the red-shifted and blue-shifted CLEANed maps (**d-c**). Contour spacing is 3.75 mJy/beam ($2.45 \text{ Jy.km.s}^{-1}$, 2σ). **f** Difference between the red-shifted and blue-shifted *dirty* maps. Same contours as **e**. The greyscale image is smoothed V band image from the HST archive data, smoothed to $0.2''$ resolution.

2. Observations and results

The observations were collected with the IRAM mm array on Plateau de Bure, using 4 antennas arranged in 3 different configurations on 1996 January 20, February 29 and April 13. The source was observed for 5, 9 and 8.5 hours respectively. An additional data set was obtained with 5 antennas on 1997 February 8, for 6 hours. The dual-frequency receivers were tuned to frequencies 97.200 GHz and 226.725 GHz , corresponding to the CO(3-2) and (7-6) transitions respectively. Typical SSB system temperatures were 150 K at 97.2 GHz and 250 to 400 K at 226.7 GHz . Two correlator units were set to cover the CO(3-2) line, with a total bandwidth of $\approx 280 \text{ MHz}$ or 850 km.s^{-1} , and 4 units were used to cover the CO(7-6) line, with a total bandwidth of 500 MHz or 660 km.s^{-1} .

The 4 configurations provided 28 baselines from 24 to 408 m , leading to beam sizes (FWHM) of $1.87'' \times 0.97''$ at PA = 23° at 97.2 GHz , and $0.77'' \times 0.44''$ at PA 15° at 226.7 GHz , using natural weighting. Amplitudes, phases and bandpasses were calibrated using 3C273 and 1413+135, and the flux density scale checked on MWC349 (flux density 0.93 Jy at 97 GHz and 1.55 Jy at 227 GHz). Both phases and amplitudes appeared to be remarkably stable during the observing runs, especially on the longest baselines where the measured phase noise was $< 40^\circ$ at 226.7 GHz .

Although the true “seeing disk” has a non-gaussian shape because of varying conditions on the 4 observing days, an effective gaussian “seeing” of FWHM $\sim 0.20''$ provides a reasonable estimate, especially with regard to flux density conservation.

3 mm results:

The Cloverleaf map in the CO(3-2) line shows elongated

Table 1. Parameters of the Cloverleaf image, positional shifts, flux ratios R, and elongations.

	HST			CO (7-6)						Model
	$\Delta\alpha$	$\Delta\delta$	R_V	$\Delta\alpha$	$\Delta\delta$	Flux	R_{CO}	Major Axis	Minor Axis	PA
A	0	0	1	0	0	12.2 (1.9)	1	0.42 (0.09)	0.32 (0.13)	23 (53)
B	0.74	0.17	0.85	0.67 (0.03)	0.15 (0.04)	13.3 (1.6)	1.09 (0.28)	0.38 (0.20)	0.2 ^a	72 (18)
C	-0.49	0.71	0.76	-0.37 (0.03)	0.63 (0.04)	12.9 (1.7)	1.06 (0.28)	0.51 (0.10)	0.24 (0.10)	6 (17)
D	0.35	1.03	0.68	0.38 (0.04)	0.98 (0.05)	6.2 (0.8)	0.50 (0.14)	0.2 ^b	0.2 ^b	n.a.

Positions and sizes axes are in $''$, fluxes in Jy. km.s^{-1} , position angle in degree. Errors are 1σ .

^a Not resolved: apparent size is $0.16 \pm 0.10''$.

^b Fixed parameters, see text.

isophotes, suggesting that the image is marginally resolved. By fitting an elliptical gaussian directly into the visibility data, we get an image size of $1.49'' \pm 0.10'' \times 1.10'' \pm 0.08''$ at PA $-68^\circ \pm 9^\circ$. The angular resolution being insufficient to separate the 4 CO(3-2) spots, we have built a model of the Cloverleaf based on the HST data (see Table 1). This model assumes for each spot a circular gaussian shape with FWHM=0.25'', and relative CO fluxes similar to those observed in the V band. Visibilities are then computed from the model using the sampling defined by the observations to produce a synthetic data set. An elliptical gaussian fit to this synthetic UV data then provides an image size of $1.29'' \times 1.00''$ at PA -56° . These values are strikingly similar to those obtained on the direct fit to the visibilities of the observed data set. In the CO(3-2) line, with a typical resolution of $1''$, the Cloverleaf is on the verge of being resolved. In other respects, the CO(3-2) line characteristics are consistent with those derived earlier (B94).

Because of the limited bandwidth, and since the receivers were tuned in single sideband to minimize system noise, this data set does not provide information on the 3mm continuum. We have used previous observations performed in November and December 1994 with a 100 MHz bandwidth on either side of the CO(3-2) line to derive an upper limit of 2.7 mJy (3σ) for the continuum at 97 GHz.

1.3 mm results:

The Cloverleaf map in the CO(7-6) line is displayed in Fig. 1. The four spots are quite conspicuous, leading to the immediate conclusion that the CO line emission is subject to gravitational lensing, as emission at other wavelengths. Before we discuss more thoroughly this image and its implications in terms of gravitational lensing, let us report on other characteristics of the observations.

In the image sideband, at frequency 229.711 GHz, we do not detect any flux (Fig. 1b), neither in the 1996 nor in the 1997 data sets. In the combined image, the rms noise is 0.95 mJy/beam. With 4 beams to cover the lensed image (i.e. assuming unresolved spots), this non-detection implies that the continuum level at 1.3 mm is < 6 mJy at the 3σ level. Using the model derived from the image in the CO(7-6) line (see Table 1), we actually measure a 1.3 mm flux of 5 ± 3 mJy (the higher rms being due to the incorporation of extended spots). Such low values show some discrepancy with the bolometer measurement of 18 mJy obtained at 1.25 mm (B95). We have considered several hypotheses to explain this discrepancy. First,

on the basis of the current CO(7-6) line intensity (see below), we have computed the contribution to the bolometer measurement of the only two CO emission lines falling in the bolometer bandpass, CO(7-6) and CO(8-7) at 258 GHz. With a CO(7-6) integrated line flux of 45 Jy.km.s^{-1} , over 650 km.s^{-1} , we get a level of 69 mJy over 500 MHz, hence, approximately 0.7 mJy over the 50 GHz bandwidth of the bolometer. Assuming that the two lines are of comparable strength, the line contribution to the bolometer measurement is at most 1.4 mJy, insufficient to explain the difference between the two measurements. Second, our lack of detection could be due to the continuum source being resolved in the interferometer map. Taking into account the interferometer baselines and the sensitivity of our experiment, the source would have to be more extended than $2''$ to escape detection, which is unlikely. Given the unambiguous detection of the CO(7-6) line in our experiment, and given the repeatability of the interferometer measurement over a one year period, we are left with the conclusion that the bolometer data is anomalously high. Such discrepancies in bolometer measurements have already been noticed for PC2132+0126 (Omont et al. 1996). Indeed, considering the continuum measures at 438 and $761 \mu\text{m}$ (B95), one derives a spectral index of 3, which, extrapolating the flux to 1.3mm, leads to a 7 mJy level prediction, consistent with the upper limit we derived. New bolometer measurements at 1.25 mm would be required to resolve the present discrepancy.

We have searched for velocity structure in the CO(7-6) maps. Because of limited sensitivity, we cannot produce individual channel maps. Instead we have extracted and combined data over the velocity ranges ($-325, -75 \text{ km.s}^{-1}$) and ($75, 325 \text{ km.s}^{-1}$) with respect to the central frequency of 226.715 GHz (redshift 2.558). The corresponding maps are shown in Fig. 1c-d, and show apparent differences. Spot B is stronger on the blue side of the line, while spot C, and marginally spot D, are enhanced on the red side. Fig. 1e presents the difference (red minus blue) between images shown in Fig. 1c-1d: no enhancement above the 3σ level is evident. Moreover, the difference image is sensitive to the deconvolution procedure. To further probe the validity of this result, especially with regard to non-linear effects in the deconvolution, we have made a difference map of the original ‘‘dirty’’ red and blue maps. This difference is displayed in Fig. 1f: no obvious signal can be identified. However, the rms noise within a $5''$ circle around the CO(7-6) emission is $\simeq 2.4$ mJy/beam, i.e. about 20% higher than the $\simeq 1.9$ mJy

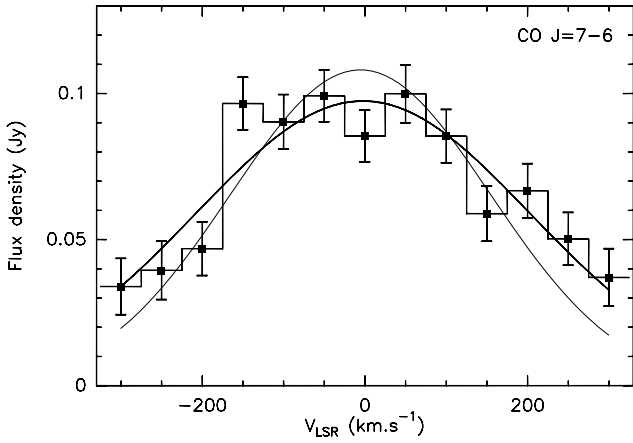


Fig. 2. Spectrum of the CO(7-6) line towards the Cloverleaf. Error bars are $\pm 1\sigma$. The thin curve corresponds to a gaussian fit with FWHM 376 km.s^{-1} , as derived from lower transitions of CO, and the thick line is the best gaussian fit to the CO(7-6) line, with FWHM 480 km.s^{-1} .

value found over the whole image. This suggests that there may be a weak signal hidden in the noise at the location of the Cloverleaf, i.e. a slight dependence of the emission on velocity.

If confirmed, such a difference in the spot pattern with velocity would require the CO source to be extended, with an intrinsic velocity gradient.

Deriving the spatially integrated line profile for weak, spatially resolved emission is a difficult task. We computed the line profile using a source model made of 4 elliptical gaussian spots, using the position and sizes derived from the integrated intensity map as discussed in Sect. 3. This procedure is justified since the velocity gradient, if any, is weak. The line profile extends over 650 km.s^{-1} and no line-free channels are accessible at the band edges (Fig. 2). The integrated line flux is $45 \pm 2 \text{ Jy.km.s}^{-1}$. By fitting a gaussian line-profile with FWHM of 376 km.s^{-1} (the mean FWHM of the other CO lines detected with the 30-m telescope, B97), we obtain $43.3 \pm 2.4 \text{ Jy.km.s}^{-1}$, and a line velocity center of $-5 \pm 14 \text{ km.s}^{-1}$. If we let the FWHM be a free parameter, we obtain FWHM = $480 \pm 35 \text{ km.s}^{-1}$ and an integrated area (over the full line) of $50.1 \pm 2.8 \text{ Jy.km.s}^{-1}$.

The larger FWHM of the CO(7-6) line with respect to lower excitation CO transitions could suggest that there is a radial gradient of the physical conditions and kinematical parameters in the warm molecular gas of the quasar (e.g. increased rotational velocity inwards).

We shall devote the rest of the discussion to the impact of the high resolution CO(7-6) map on the modeling of the lens and the knowledge of the quasar molecular content.

3. Discussion

The integrated CO(7-6) map, restored with a circular $0.5''$ beam is shown in Fig. 3.

We have chosen to compare our image with a V band image available from the HST archive, because of the high relative astrometric precision obtained in both cases ($\sim 0.02''$ for the HST, and $\sim 0.04''$ for our data). On the V band HST image, the

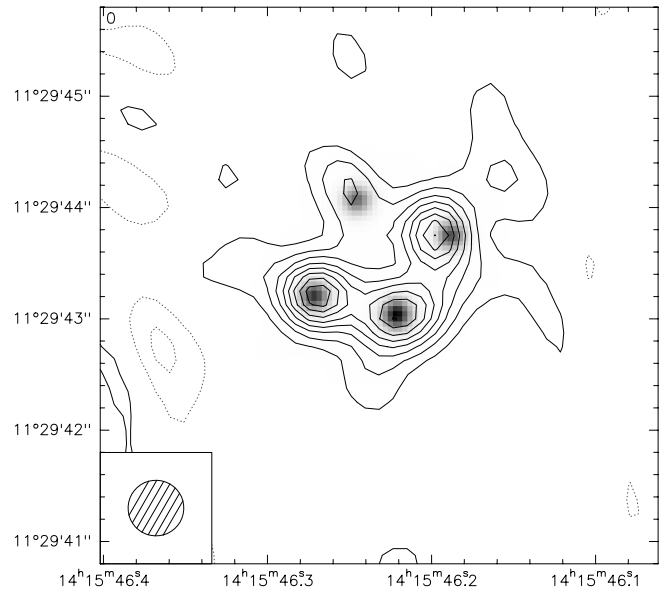


Fig. 3. The integrated CLEANed CO(7-6) map restored with a circular beam of $0.5''$. Contour spacing is 1.65 mJy/beam (corresponding to 1.1 Jy.km.s^{-1}) i.e. 2σ . The greyscale image is one of the V band image from the HST archive data, smoothed to $0.2''$.

4 spots appear circular, demonstrating that they are related to a point-like component in the quasar. Their positions and intensity ratios, arbitrarily referred to spot A, are provided in Table 1.

For the modeling of the CO(7-6) image, we have performed all measurements -spot flux ratios or sizes- through a fitting procedure in the visibility domain, in order to avoid possible spurious effects of the deconvolution procedure. We consider a model with 4 gaussian spots, having either a circular or an elliptical shape.

The positions of the spots were derived assuming a circular gaussian with FWHM = $0.30''$ (larger than the seeing value). Once the positions were determined, the sizes were first measured by fitting circular gaussians at the fixed positions. Spots A, B and C appeared to have an extension larger than the seeing value, while spot D is too weak to be analysed in this way. Therefore, in a last step, we fixed as well the size of spot D to $0.2''$, and allowed the 3 other spots to have elliptical gaussian shapes. Final sizes, corrected for the seeing value, are given in Table 1.

At a level of 3σ , we find that spots B and C are stretched along the Einstein ring by a factor ~ 2 . In addition, we observe that the separations of the A,B,C spot pairs are smaller in CO than in the optical, especially for the pairs involving spot C. This shows that some of the CO spots are displaced by $\simeq 0.1''$ with respect to the Einstein ring defined by the optical positions.

Although the lens itself is not detected in the Cloverleaf, K90 have worked out a detailed model of the lensing system. They assume the deflector to be at $z=1.44$, the redshift of a narrow absorption line system, and consider two possible shapes, a single elliptical singular isothermal galaxy or 2 spherical singular isothermal galaxies. Both shapes are consistent with the

radio and R band data. For the sake of simplicity, we shall retain the former. According to their model, the centre of the deflector is $0.6''$ off the line of sight to the core of the quasar. Then, the quasar falls within the diamond caustic of the lens, producing 4 detectable images, the fifth one near the centre being too faint.

We find flux ratios among the CO spots to be comparable (within the uncertainties) to those derived in the other wavebands. However, the K90 model does not properly reproduce the observed flux ratios (and did not intend to do so since only geometrical parameters were fitted). Pending an improved modeling of the lensing system, a total total amplification factor of 7.6 has to be retained in deriving the molecular content from the observed CO lines (B97).

According to the theory, (see for example Narayan & Grossman 1988 as well as Burke et al. 1991), in a lens configuration similar to that of the Cloverleaf, the core of the quasar would produce 4 concentrated spots located on the Einstein ring, while an extended source around the core would produce 4 spots stretched along the Einstein ring (see Burke et al. 1991, Fig. 2d). Indeed, we observe that some of the CO(7-6) spots in the Cloverleaf are stretched with respect to their optical counterparts, leading us to conclude that the CO source is extended in the quasar. Moreover, being extended, different parts of the CO source are approaching different sides of the caustic of the lens, causing an ensemble of spot displacements: an inward or outward shift of the spots with respect to the Einstein ring, and shifts along the ring. The absolute astrometric accuracy of the HST ($0.3''$) and CO ($0.1''$) images does not allow sufficiently precise registration to directly measure the inward and outward displacements.

Combining the CO observations and the available Cloverleaf model of K90, we can derive an estimate of the size of the CO source in the quasar. The CO source is not likely crossing the diamond caustic, otherwise the changes of the image pattern on the CO map would be more dramatic. Therefore, an upper limit of 600 pc ($0.12''$) for the CO source radius in the quasar, would seem a reasonable estimate (see K90, Fig4b). An improved model of the lens, incorporating the new constraints

contained in the CO map, in particular the flux ratios which are free of microlensing effects, should be worked out before we can derive a more precise value. Such a study is beyond the scope of this paper. The 600 pc size of the CO emitting region, together with the total magnification of 7.6, leads to a dynamical mass of $510^9 M_{\odot}$ (see B97 for the derivation).

Acknowledgements. We are gratefully indebted to the IRAM staff members who performed the observations on Plateau de Bure, as well as to P.Maloney and T.Hurt for interesting discussions.

References

- Angonin M.C., Remy M., Surdej J., Vandierriest C., 1990, *A&A* 233, L5
- Arnould P., Remy M., Gosset E., et al. 1993, in "Gravitational Lenses in the Universe", eds. J.Surdej et al. , Université de Liège, p.169
- Barvainis R., Tacconi L., Antonucci R., Alloin D., Coleman P., 1994, *Nat* 371, 586 (B94)
- Barvainis R., Antonucci R., Hurt T., Coleman P., Reuter H., 1995, *ApJ* 451, L9 (B95)
- Barvainis R., Maloney P., Antonucci R., Alloin D., 1997, *ApJ* in press, (B97)
- Burke B.F., Lehar J., Conner S.R., 1991, in "Lecture Notes in Physics", eds. R.Kayser, T.Schramm & L.Nieser, Springer-Verlag, p237
- Falco E.E., 1993, in "Gravitational Lenses in the Universe", eds. J.Surdej et al. , Université de Liège, p.127
- Kayser R., Surdej J., Condon J.J., et al. 1990, *ApJ* 364, 15 (K90)
- Lawrence C.R., 1996, in "Astrophysical Applications of Gravitational Lensing", eds. C.Kochanek & J.Hewitt, Kluwer, p.299
- Magain P., Surdej J., Swings J.P., et al. 1988, *Nat* 334, 325
- Omont A., McMahon R.G., Cox P., et al. 1996, *A&A* 315, 1
- Remy M., Gosset E., Hutsemekers D., et al. 1996, in "Astrophysical Applications of Gravitational Lensing", eds. C.Kochanek & J.Hewitt, Kluwer, p.261
- Scoville N.Z., Yun M.S., Bryant P.M., 1996 in "Cold gas at high redshift", Bremer et al. (eds.), Kluwer Academic Publishers, p25.
- Wilner D.J., Zhao J.-H., Ho P.T.P., 1995, *ApJ* 453, L91